Pressure tensor of the hard-disk Lorentz gas

Janka Petravic
Research School of Chemistry, The Australian National University, Canberra, Australian Capital Territory 0200, Australia

Dennis J. Isbister
Department of Physics, University College, University of New South Wales, Australian Defence Force Academy, Canberra, Australian Capital Territory 2600, Australia

(Received 28 November 1994)

The exact solutions of the hard-disk collisions obeying Sllod dynamics (so named because of its close relationship to the Dolls tensor algorithm) with isoenergetic and isokinetic constraints have been presented and discussed. In equilibrium the trajectories in the isokinetic and isoenergetic systems are indistinguishable, but the pressures are not equal. Outside equilibrium, with a shear present, the isoenergetic constraint is shown to be inappropriate for the Lorentz model. The solution of the isokinetic hard-disk collision has been used to evaluate and qualitatively explain the dependence of the potential part of the pressure tensor on shear rate. The hard-disk results have been compared to the results for soft disks.

PACS number(s): 05.20.Dd

I. INTRODUCTION

The two-dimensional Lorentz model is the simplest possible model of shear flow. It consists of two particles in a periodic cell with the Lees-Edwards moving periodic boundary conditions [1], obeying the Sllod [2] equations of motion. The reference frame of the system is fixed on one of the particles, the scatterer of radius σ, while the motion of the moving point particle of the reduced mass $m/2$ and momentum $\mathbf{p}$ is described by the equations of motion,

$$\dot{x}=2p_x/m+\gamma y\ ,\quad \dot{p}_x=F_x-\gamma p_y-\alpha p_x\ ,$$
$$\dot{y}=2p_y/m\ ,\quad \dot{p}_y=F_y-\alpha p_y\ . \tag{1}$$

The force $\mathbf{F}$ is the conservative force of interaction between the disks, and γ is the applied shear rate. The Sllod algorithm (so named because of its close relationship to the Dolls tensor algorithm) correctly incorporates the coupling to the external shearing field, which results in streaming velocity of a constant gradient being superimposed on the peculiar velocities of the particles, and thus prevents the attainment of an equilibrium state. The external field continuously performs work on the system. If a nonequilibrium steady state is to be achieved, a constraint ("friction") coefficient α has to be introduced. This factor can be defined in such a way that the heat generated by the external field is removed or added, keeping the peculiar kinetic energy p^2/m conserved ("isokinetic constraint"). The other definition of α can be such that the excess energy created by the external field is compensated, and the total peculiar energy $E=p^2/m+U(r)$ is conserved at all times ("isoenergetic constraint"), where $U(r)$ is the potential energy generating the conservative repulsive force of interaction $\mathbf{F}$.

In the former case, the isokinetic constraint or the "Gaussian thermostat" is given by $\alpha=\alpha_K$,

$$\alpha_K=(\mathbf{F}\cdot\mathbf{p}-\gamma p_x p_y)/p^2\ , \tag{2}$$

ensuring that the magnitude of the momentum is conserved at all times. In the latter isoenergetic case $\alpha=\alpha_E$, where

$$\alpha_E=-\gamma\left[\frac{mFxy}{2r}+p_x p_y\right]\Big/p^2\ . \tag{3}$$

In the regions of space where there is no interaction between the point particle and the scatterer, i.e., where $\mathbf{F}=\mathbf{0}$, the isokinetic and isoenergetic constraint coefficients α_K and α_E coincide because both the conservation of kinetic and total energy mean that the magnitude of the momentum p remains unchanged. The system (1) and (2) or (1) and (3) then can be solved in terms of three variables, the position coordinates of the moving particle (x,y) and the angle θ between the momentum $\mathbf{p}$ and the x axis. Between the collisions the equations of motion for these variables are

$$\dot{x}=\frac{2p}{m}\cos\theta+\gamma y\ ,\quad \dot{y}=\frac{2p}{m}\sin\theta\ ,\quad \dot{\theta}=\gamma\sin^2\theta\ , \tag{4}$$

which can be solved analytically [3].

The Lorentz model has served to study the most elementary features of nonequilibrium steady states of shear flow. It is simple enough for many of its properties to be understood theoretically, while it still exhibits the characteristics of real nonequilibrium sheared fluids like shear thinning, shear dilatancy, and normal stress difference.

The microscopic expression for the components of the pressure tensor of the Lorentz gas is given as a time average,

$$P_{\alpha,\beta}=\frac{1}{V}\left\langle 2\frac{p_\alpha p_\beta}{m}+r_\alpha F_\beta\right\rangle$$
$$=\lim_{t\to\infty}\frac{1}{Vt}\left[\int_0^t 2\frac{p_\alpha(s)p_\beta(s)}{m}ds+\int_0^t r_\alpha(s)F_\beta(s)ds\right],$$
$$\text{where } \alpha,\beta=x,y \ . \quad (5)$$

The first term on the right-hand side (rhs) of (5) is the kinetic part of the pressure tensor, which gives the contribution of the motion of the point particle to the momentum flux. The second term is the potential part of the pressure tensor, which describes the momentum transfer due to the interaction with the scatterer during collisions.

For hard disks the contribution to the kinetic part comes only from the motion of the moving (point) particle between the collisions, and it depends only on the distribution of the average direction of momentum between the collisions. The analytic solution of the Sllod equations between the collisions was used to obtain the steady-state distribution of the polar angle of the momentum from the relaxation time approximation of the Boltzmann equation, using the assumption that the velocity distribution function f depends only on the angle θ of the momentum and is uniform in all the other variables. The derivation uses only the last equation of (4) and does not depend on the type of applied constraint. The steady-state solution of the Boltzmann equation [3,4] can predict the dependence of the kinetic part of the elements of the pressure tensor on shear rate with a quite good correspondence to the simulation results, implying that the only parameter responsible for the behavior of the kinetic part of the pressure tensor is $\gamma\tau_R$, where τ_R is the density (and shear rate) dependent "relaxation time." The consequence of this solution is that the kinetic part of the pressure tensor does not depend on density and shear rate as separate parameters. It has been therefore assumed that the steady state of the hard-disk Lorentz gas can be characterized by only one parameter, $\gamma\tau_R$, and that it is sufficient to find the dependence of the steady state on shear rate for one density to characterize all possible steady states.

The discrepancies between the predictions of the solution of the Boltzmann equation and the simulation results for the kinetic part of the pressure tensor of the thermostated Lorentz gas arise from the fact that the velocity distribution function f depends also on position (x,y) and explicitly on time. The importance of the periodic time dependence, introduced by the Lees-Edwards boundary conditions, for the characterization of steady state has first been emphasized by Hoover *et al.* [10], and is discussed in Ref. [5].

The potential contributions to the hard-disk Lorentz gas pressure tensor are the impulses received by the moving particle in the time intervals of vanishing duration. If n collisions of infinitesimal duration ε occur at times t_i $(i=1,\ldots,n)$ during the total elapsed time t, the potential part of the hard-disk Lorentz gas is

$$P_{\alpha,\beta}^{\text{potential}}=\frac{1}{Vt}\sum_{i=1}^{n}\lim_{\varepsilon\to 0}\int_{t_i}^{t_i+\varepsilon} r_{\alpha i}(s)F_{\beta i}(s)ds \ . \quad (6)$$

In the limit when $F\to\infty$, $\varepsilon\to 0$ (hard-disk limit) the integrals in (6) for the ith collision become

$$\lim_{\substack{F\to\infty\\ \varepsilon\to 0}}\int_{t_i}^{t_i+\varepsilon} r_{xi}(s)F_{xi}(s)ds=\sigma A_i\cos^2\varphi_i \ ,$$
$$\lim_{\substack{F\to\infty\\ \varepsilon\to 0}}\int_{t_i}^{t_i+\varepsilon} r_{xi}(s)F_{yi}(s)ds=\sigma A_i\cos\varphi_i\sin\varphi_i \ , \quad (7)$$
$$\lim_{\substack{F\to\infty\\ \varepsilon\to 0}}\int_{t_i}^{t_i+\varepsilon} r_{yi}(s)F_{yi}(s)s=\sigma A_i\sin^2\varphi_i \ ,$$

where φ_i is the polar angle of the position of the moving particle at the ith collision (Fig. 1) and A_i is the collision impulse

$$A_i=\lim_{\substack{F\to\infty\\ \varepsilon\to 0}} F\varepsilon \ . \quad (8)$$

The collisions of hard disks in sheared hard-disk Lorentz gas were conventionally simulated using some stiff repulsive interaction potential, like a stiff Hooke's law. Recently an analytic solution for the instantaneous change of θ in the thermostated hard-disk collision under shear has been presented [5]. The solution has been obtained using a generalization of a method outlined in [6] for the Evans-Gillan model of heat flow. In this paper the solution from [5] is reviewed, and its implications for the potential part of the pressure tensor are discussed for both the equilibrium and nonequilibrium cases. The same method applied to a sheared isoenergetic collision shows that the isoenergetic constraint cannot be used in the hard-disk approximation.

II. EQUILIBRIUM CASE

A. Collisions

In equilibrium, i.e., when $\gamma=0$, the isoenergetic constraint vanishes and the equations of motion of the point particle with the total energy conserved are

$$\dot{x}=2p_x/m \ , \quad \dot{p}_x=Fx/r \ ,$$
$$\dot{y}=2p_y/m \ , \quad \dot{p}_y=Fy/r \ , \quad (9)$$

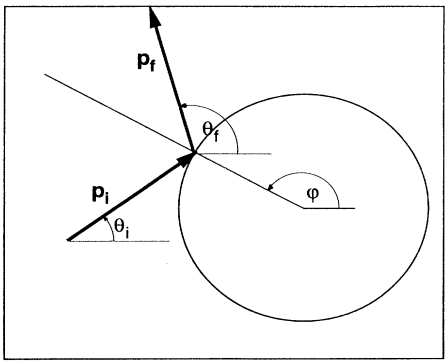

FIG. 1. Definition of angles characterizing a hard-disk collision. The angle θ_i is the angle between momentum and the x axis just before the collision, θ_f is the angle between momentum and the x axis just after the collision, and φ is the polar angle of the position of the point of collision.

while the thermostated "isokinetic" equations of motion that conserve the kinetic energy are

$$\dot{x}=2p_x/m\ ,\quad \dot{p}_x=Fx/r-\mathbf{F}\cdot\mathbf{p}p_x/p^2\ ,$$
$$\dot{y}=2p_y/m\ ,\quad \dot{p}_y=Fy/r-\mathbf{F}\cdot\mathbf{p}p_y/p^2\ . \tag{10}$$

In order to find the behavior of the point particle during a hard-disk collision we shall follow the method outlined in [6] and [5]. In this method the constant radial repulsive force is allowed to increase to infinity, causing the time of collision ε (while the point particle is inside the scatterer) to tend to zero, keeping the product $F\varepsilon$ finite. The length of the infinitely short time interval ε is determined by the condition that the scatterer be circular, i.e, that the distance to the origin at the beginning and at the end of collision has to be equal to σ.

Because the direction of the force $\mathbf{F}$ is radial, the equations of motion for the rate of change of the momentum are first written in terms of the radial and tangential components, and in the hard-disk limit ($F\to\infty$) all the terms not containing F are neglected. Therefore in the hard-disk limit the momentum equations become

$$\text{Isoenergetic:}\quad \dot{p}_r=F,\quad \dot{p}_t=0\ , \tag{11}$$

$$\text{Isokinetic:}\quad \dot{p}_r=F\left[1-\frac{p_r^2}{p^2}\right]\ ,\quad \dot{p}_t=\frac{F}{p^2}p_rp_t\ . \tag{12}$$

The solutions for the radial and tangential components are [5]

$$\text{Isoenergetic:}\quad p_r(t)=p_{ri}+F(t-\varepsilon_1),\quad p_t(t)=p_{ti}\ , \tag{13}$$

$$\text{Isokinetic:}\quad p_r(t)=p\tanh(Ft/p)\ ,\quad p_t(t)=p/\cosh(Ft/p)\ , \tag{14}$$

where p_{ri} and p_{ti} are the initial radial and tangential components at the "beginning of collision" and ε_1 is the time of the beginning of collision.

The final momentum at the "end of collision" is determined from the condition that the radial distances traveled before and after the turning point be equal,

$$\Delta r=\int_{\varepsilon_1}^{\varepsilon_2}\dot{r}(t)dt=\int_{\varepsilon_1}^{\varepsilon_2}\frac{2p_r}{m}dt=0\ , \tag{15}$$

where ε_2 is the time of the end of collision such that $\varepsilon=\varepsilon_2-\varepsilon_1$. This gives for both types of collisions the total change of radial and tangential components of momentum

$$\Delta p_r=p_{rf}-p_{ri}=-2p_{ri}\ ,\quad \Delta p_t=0\ , \tag{16}$$

where p_{rf} and p_{tf} are the final radial and tangential components at the end of collision.

It can be observed that for the thermostated disks, when the force $\mathbf{F}$ between the disks is finite and the point particle collides with the scatterer totally radially ($p_{ri}=p$), the complete equation of motion for the radial component shows that the rate of change of momentum is identically zero,

$$\dot{p}_r=F\left[1-\frac{p^2}{p_r^2}\right]+\frac{2p^2}{mr}-\frac{2pp_r}{mr}\equiv 0\ . \tag{17}$$

The point particle goes right through the scatterer without any change in momentum. The physical reason for such behavior is that in the thermostated system with the isokinetic constraint (2) the momentum of the point particle is allowed to change its direction but not its magnitude. Therefore during a collision the momentum rotates in the sense determined by this initial tangential component. When there is no tangential component, it "cannot decide" in which sense to rotate and the initially radial momentum remains unchanged during a thermostated collision.

When the force in (17) tends to infinity, the rhs of (17) becomes undetermined and the final momentum has to be found as a limiting case of "nearly radial" trajectories, i.e., again as $p_{rf}=-p_{ri}=p$, as predicted by (16).

B. Potential part of the pressure tensor

A hard-disk collision can be characterized by the angles θ_i, the angle between momentum and the x axis just before the collision, and φ, the polar angle of the position of the collision point (Fig. 1). The angle between momentum and the x axis just after the collision is θ_f. As the system in equilibrium is isotropic, the impulse A depends only on the difference $\theta_i-\varphi$,

$$\text{Isoenergetic:}\quad A_i=-2p_{ri}=-2p\cos(\theta_i-\varphi)\ , \tag{18}$$

$$\text{Isokinetic:}\quad A_i=p\ln\frac{1-p_{ri}/p}{1+p_{ri}/p}=p\ln\frac{1-\cos(\theta_i-\varphi)}{1+\cos(\theta_i-\varphi)}\ . \tag{19}$$

The change of momentum in an isokinetic hard-disk collision is equal to the change of momentum in an isoenergetic hard-disk collision, and both collisions occur in an infinitely short time. However, the ratio of the collision time intervals of isoenergetic to isokinetic collisions is always less than unity (see Fig. 2). Isokinetic collision takes longer, even in the hard-disk limit, and the isokinetic impulse (19) is therefore larger than the isoenergetic impulse (18) and becomes singular for the totally radial initial momentum.

The values of the thermostated collision impulse

$$A=\int_{\varepsilon_1}^{\varepsilon_2}F\,dt$$

obtained by numerical simulations for the increasing constant force, the stiff spring with increasing elasticity constant, and the truncated Lennard-Jones potential with increasing well depth all approach the value predicted by (19) for hard disks.

In equilibrium, when all possible collisions (i.e., all possible combinations of angles θ_i and φ) are equally probable, the ratio of the potential parts of pressure is equal to the ratio of the shaded areas in Fig. 2,

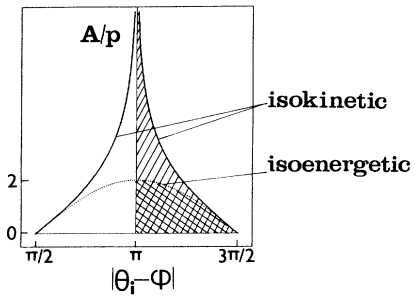

FIG. 2. Isoenergetic and isokinetic impulse $A(\theta_i-\varphi)$ in the equilibrium collision as a function of the angles θ_i and φ before the collision at $r=\sigma$ (shaded region). The isokinetic collision is singular for $\theta_i-\varphi=\pm\pi$. The ratio of the impulses is the ratio of the shaded areas.

$$\frac{P^{\text{potential}}_{\text{isokinetic}}}{P^{\text{potential}}_{\text{isoenergetic}}}=\frac{\int_{\pi/2}^{\pi}d(\theta_i-\varphi)\ln\frac{1-\cos(\theta_i-\varphi)}{1+\cos(\theta_i-\varphi)}}{2\int_{\pi/2}^{\pi}d(\theta_i-\varphi)\cos(\theta_i-\varphi)}$$
$$=2\left[1-\frac{1}{3^2}+\frac{1}{5^2}-\cdots\right]=1.831\,94\ , \qquad (20)$$

i.e., twice Catalan's constant. This result is consistent with findings of Kratky and Hoover [6] for the heat flow model in the limit when $\lambda\to 0$.

III. ISOENERGETIC CASE WITH SHEAR

Outside equilibrium, when $\gamma\neq 0$, the equations of motion with the isoenergetic constraint are given by (1) and (3). The equations of motion for the squared components of momentum during a hard-disk collision are obtained by neglecting all the terms that do not contain F and by taking into account that during a hard-disk collision the change of momentum occurs at one point, the point of collision (x_0,y_0) at $r=\sigma$,

$$\frac{d}{dt}p_r^2=2p_r\dot{p}_r=2F\left[p_r+\frac{m\gamma x_0y_0}{2\sigma}\frac{p_r}{p_r^2+p_t^2}\right]\ , \qquad (21)$$

$$\frac{d}{dt}p_t^2=2p_t\dot{p}_t=2F\frac{m\gamma x_0y_0}{2\sigma}\frac{p_t}{p_r^2+p_t^2}\ , \qquad (22)$$

$$\frac{d}{dt}p^2=2p\dot{p}=2F\left[p_r+\frac{m\gamma x_0y_0}{2\sigma}\right]\ . \qquad (23)$$

The condition that determines the final radial component of momentum p_{rf} is

$$\Delta r=\int_{\varepsilon_1}^{\varepsilon_2}\dot{r}(t)dt=0\ .$$

With the presence of shear the radial component of the velocity of the point particle is a sum of two terms, the peculiar part $2p_r/m$ directly proportional to the radial component of peculiar momentum p_r and the radial component of streaming velocity at the point of collision $\gamma x_0y_0/\sigma$, where x_0 and y_0 are coordinates of the point of collision. Therefore in this case the boundary condition determining the final value of p_r is

$$\Delta r=\int_{\varepsilon_1}^{\varepsilon_2}\left[\frac{2p_r}{m}+\frac{\gamma x_0y_0}{\sigma}\right]dt=0\ , \qquad (24)$$

different from (15) and the condition described in [6]. From Eq. (23) it then follows that in the isoenergetic case the condition $\Delta r=0$ is equivalent to the requirement that the magnitude of momentum p at the end of collision equal the magnitude of momentum at the beginning of collision, $\Delta p=0$.

From the form of Eqs. (21), (22), and (23) it is possible to show that for each polar angle of collision φ there exists an interval of initial angles of momentum θ_i such that the collision cannot be solved. Here we present the arguments that apply to φ in the second or fourth quadrant.

From Eq. (23) it can be deduced that the minimum of kinetic energy (i.e., $p^2=p_r^2+p_t^2$) is at the turning point, when $p_r=p_{rtp}$,

$$p_{rtp}=-\frac{m\gamma x_0y_0}{2\sigma}\ . \qquad (25)$$

In the second and fourth quadrants the constant $(m\gamma x_0y_0)/(2\sigma)$ is negative. During a collision the point particle moves towards the center of the scatterer, while the radial momentum increases from the negative value p_{ri} to zero and then to the positive value p_{rtp} at the turning point.

Equation (22) states that the square of the tangential component decreases steadily from p_{ti}^2 during a collision in the second or fourth quadrant because the rhs of (22) is negative. When $p_r=0$, the square of the tangential component p_t^2 must therefore be less than the square of the tangential component p_{ti}^2 at the beginning of collision. A direct consequence is that, when $p_r=0$, the square of the *total* momentum p^2 is less than p_{ti}^2.

However, p^2 has the minimum not when $p_r^2=0$, but when $p_r^2=p_{rtp}^2$. Therefore $p^2=p_{tp}^2$ at the turning point must be less than p^2 when $p_r=0$,

$$p_{tp}^2=p_{ttp}^2+p_{rtp}^2=p_{ttp}^2+\left[\frac{m\gamma x_0y_0}{2\sigma}\right]^2<p_{ti}^2$$

and

$$p_{ttp}^2<p_{ti}^2-\left[\frac{m\gamma x_0y_0}{2\sigma}\right]^2\ . \qquad (26)$$

Condition (26) cannot be fulfilled if the rhs of the inequality is negative. If (26) is written in terms of the angles θ_i and φ, the solution of

$$|\sin(\theta_i-\varphi)|<\frac{m\gamma\sigma}{p_i}|\sin 2\varphi|\ , \qquad (27)$$

where p_i is the momentum at the beginning of the collision, yields the interval of $(\theta_i-\varphi)$ for which the collision cannot be solved. For every angle of collision $\varphi\neq k\pi/2$, where k is an integer, such an interval has nonvanishing length (see Fig. 3).

Condition (27) can be obtained for the collisions in the first and third quadrants of φ following a similar type of argument. This means that if the isoenergetic constraint

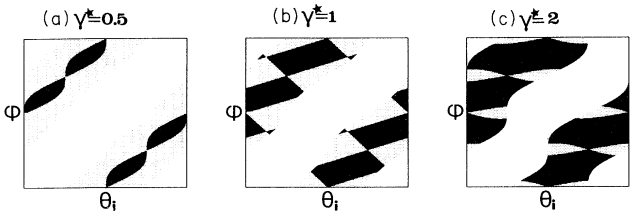

FIG. 3. Distribution of angles θ_i and φ at $r=\sigma$ characterizing a hard-disk collision can be represented in the (θ_i,φ) plane. The momentum angle $\theta_i \in [0,2\pi]$ is plotted on the abscissa, whereas the angle of the collision point $\varphi \in [0,2\pi]$ is plotted on the ordinate. The gray regions represent all possible pairs (θ_i,φ) (i.e., corresponding to $\dot{r}<0$) for three values of reduced shear rate. The black regions around the radial direction represent the pairs (θ_i,φ), for which the inequality (27) holds. An isoenergetic hard-disk collision cannot be solved *at least* in these regions.

is used, a finite fraction of hard-disk collisions cannot be solved.

IV. ISOKINETIC CASE WITH SHEAR

A. Collisions

When $\gamma \neq 0$, the equations of motion with the isokinetic constraint are given by (1) and (2). In the hard-disk limit the collision is solved using the same limiting procedure as was used in solving the equilibrium isokinetic collision. The momentum is resolved into its radial and tangential components, and the terms that do not contain the infinite force **F** are discarded. Thus, obtained equations of motion are identical to Eqs. (12), describing the equilibrium isokinetic collision, and give the same time dependence (14) of the radial and tangential components of momentum. The condition that determines the final radial component of momentum p_{rf} is given by (24). Therefore the final value of momentum is determined from

$$\Delta r = \int_{\varepsilon_1}^{\varepsilon_2} \left[\frac{2p_r}{m} + \frac{\gamma x_0 y_0}{\sigma} \right] dt = \int_{\varepsilon_1}^{\varepsilon_2} \left[\frac{2p}{m} \tanh\left[\frac{Ft}{p} \right] + \frac{\gamma x_0 y_0}{\sigma} \right] dt = 0 \ . \quad (28)$$

The dependence of the direction of momentum after the collision on shear rate comes from this condition. The value of the radial component of momentum after the collision is determined as a zero of the equation

$$\ln\left[\frac{1-p_{rf}^2/p^2}{1-p_{ri}^2/p^2} \right] + \frac{m\gamma x_0 y_0}{2\sigma p} \ln\left[\frac{(1+p_{rf}/p)(1-p_{ri}/p)}{(1-p_{rf}/p)(1+p_{ri}/p)} \right] = 0 \ , \quad (29)$$

using numerical methods.

A geometric interpretation of the solution of (29) is presented in Fig. 4. At the turning point of a trajectory, $\dot{r}=0$ and $p_r = p_{rtp}$, as given by (25). Condition (28) then means that on the graph of $p_r(Ft)$ the area below the line $p_r = p_{rtp} = -(m\gamma x_0 y_0)/(2\sigma)$ must equal the area above this line (i.e., the distance traveled towards the center of the scatterer must equal the distance traveled away from the center). If the collision occurs in the second or fourth quadrant of the angle φ [Fig. 4(a)], where the streaming velocity pushes the point particle further into the scatterer, p_r at the turning point is positive and the direction of the final momentum is closer to radial. When the collision is in the first or third quadrant [Fig. 4(b)], the streaming velocity pushes the point particle out of the scatterer and p_r at the turning point is negative, so that the final momentum is "less radial" than the initial momentum.

If $p_{rtp} = -(m\gamma a x_0 y_0)/(2\sigma)$ is larger than the magnitude of the momentum p [Fig. 4(a)], the $p_r(Ft)$ curve will lie entirely below the line $p_r = p_{rtp}$ and it will not be possible to solve the collision. An interval of such "forbidden" angles of collision φ appears in the second and fourth quadrants when the reduced shear rate

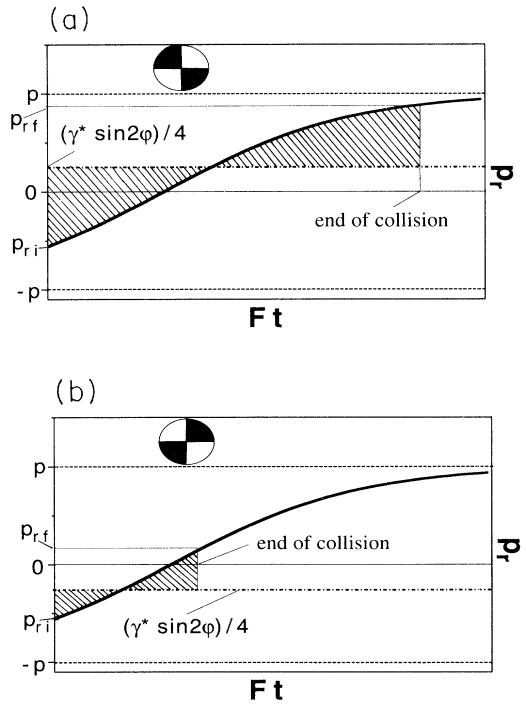

FIG. 4. (a) Change of the radial component of momentum p_r during a collision in the second or fourth quadrants of φ, shown in black in the inset. For these collisions the turning point $p_r = -m\gamma x_0 y_0/(2\sigma)$ is positive, and the condition of equality of the shaded areas below and above the turning point implies that the momentum after the collision will have a larger radial component than before the collision (i.e., $|p_{rf}| > |p_{ri}|$). (b) Change of the radial component of momentum p_r during a collision in the first or third quadrants of φ. Here the turning point $p_r = -m\gamma x_0 y_0/(2\sigma)$ is negative, and the condition that the shaded areas must be equal means that the radial component of momentum after the collision is smaller than before the collision ($|p_{rf}| < |p_{ri}|$).

$\gamma^*=m\gamma\sigma/p$ exceeds 4. For a collision occurring in this "forbidden" interval of φ, the moving particle cannot "bounce off" after the collision, but stays bound indefinitely to the scatterer. These collisions have the same origin as the artificial string phase observed in the strongly sheared soft-disk systems [7,8] with a profile-biased thermostat [8]. Therefore $\gamma^*=4$ can be considered as a limit of applicability of a linear profile thermostat. This effect is discussed in more detail in Ref. [5].

B. Potential part of the pressure tensor

Once p_{rf} has been evaluated from (29), the impulse $A(\theta_i,\varphi)$ can be found from

$$A(\theta_i,\varphi)=\frac{p}{2}\ln\frac{(1+p_{rf}/p)(1-p_{ri}/p)}{(1-p_{rf}/p)(1+p_{ri}/p)} . \tag{30}$$

Let us compare the impulse for two collisions with the same radial component of momentum at the symmetric positions in the first quadrant (at a collision angle φ) and in the second quadrant (collision angle π-φ).

Without shear the two impulses would be the same. As the shear rate increases, the impulse in the second (and the corresponding impulse in the fourth) quadrant increases [Fig. 4(a)], while the impulse in the first (and third) quadrant decreases [Fig. 4(b)]. In the former case the streaming velocity pushes the point particle into the scatterer even when the radial component of momentum is zero, and in the latter case the point particle is pushed away from the center while its radial component of momentum is still pointing towards the center of the scatterer. Therefore, even in the limit when the time of collision tends to zero, the particle spends more time within the scatterer if the collision is taking place in the second and fourth quadrants than if it is happening in the first or the third. The difference between the two impulses increases with the shear rate.

The dependence of the impulse $A(\theta_i,\varphi)$ on the positions of collision and on the reduced shear rate $\gamma^*=m\gamma\sigma/p$ is shown in Fig. 5. The contribution of a particular collision, characterized by angles θ_i and φ, to the potential part of the pressure tensor, is determined by the probability $f^\sigma(\theta_i,\varphi)$ for such a collision to occur, and, in addition, by three competing effects (Fig. 5):

(i) the increase of the impulse $A(\theta_i,\varphi)$ with shear rate in the second and fourth quadrants of φ and its decrease with γ^* in the first and third quadrants of φ;

(ii) the decrease of the impulse with the increase in the distance of $|\theta_i-\varphi|$ from the (singular) maximum at $\pm\pi$;

(iii) the value of $\cos\varphi\sin\varphi$, $\cos^2\varphi$, and $\sin^2\varphi$ at the collision which specifies the elements P_{xy}, P_{xx}, and P_{yy} of the potential part of the pressure tensor.

The probability distribution $f^\sigma(\theta_i,\varphi)$ gives the probability for the point particle to have the momentum angle θ_i at the position characterized by the polar angle φ at the circumference of the scatterer $r=\sigma$ just *before a collision.* This distribution depends on both reduced density $\rho^*=\rho\sigma^2$ and reduced shear rate γ^*. The probability distributions for two values of shear rate $\gamma^*=1$ and $\gamma^*=3$ and for two densities ρ^* are shown in Fig. 6.

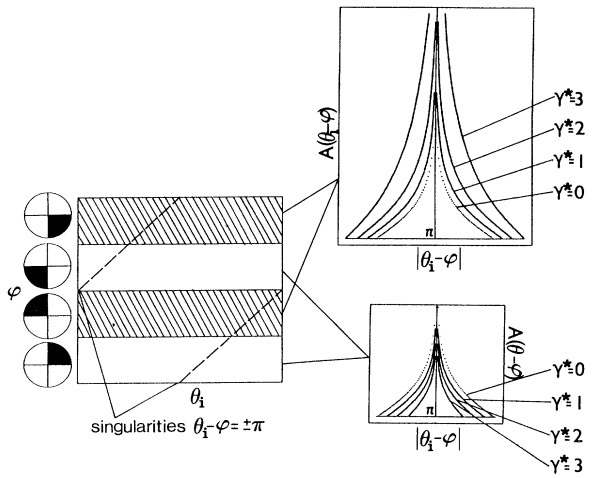

FIG. 5. Competing effects determining the dependence of the average collision impulse on shear rate. The square in the middle of the picture represents the (θ_i,φ) plane at the collision $(r=\sigma)$. The square is divided into four intervals of φ corresponding to the quadrants shown in black on the left-hand side of the picture. In the second and fourth (shaded) quadrants the collision impulse $A(\theta_i,\varphi)$ (where θ_i is the momentum angle at $r=\sigma$ before the collision) increases with γ^* with respect to the equilibrium value, while in the first and third (unshaded) quadrants it decreases. The impulse always has a singular maximum on the dashed line $\theta_i-\varphi=\pm\pi$. The average impulse $\langle A(\theta_i,\varphi)\rangle$ for an angular distribution of φ and θ_i before the collision at $r=\sigma$ will be determined from the position of the maximum of the probability distribution in the (θ_i,φ) plane: whether it is in the shaded or in the unshaded region, and how far it is from the dashed line.

In order to represent the distribution of angles just *before a collision,* the distribution function $f^\sigma(\theta_i,\varphi)$ can be nonzero only for such pairs of angles (θ_i,φ) for which the motion of the point particle is towards the center of the scatterer, i.e., where $\dot r<0$, so that

$$\dot r(\theta_i,\varphi)=\frac{2p}{m}\cos(\theta_i-\varphi)+\frac{\gamma\sigma}{2}\sin2\varphi<0 . \tag{31}$$

These are the regions of the angles θ_i and φ over which we have to average the impulse $A(\theta_i,\varphi)$ to obtain the potential part of the pressure tensor. From Eq. (31) and Fig. 6 it can be seen that the shape of these regions depends only on reduced shear rate γ^* and not on density ρ^*.

The probability density of a certain collision characterized by a pair (θ_i,φ) in these regions depends both on density and shear rate:

(i) the increase in shear rate makes the angle θ between the collisions rotate faster towards 0 or π [last equation of (4)], causing the most probable values of the angle θ_i at the end of a "free" trajectory to get close to 0 or π with the increase in shear rate;

(ii) the decrease in density at constant shear rate increases the average time between the collisions and allows

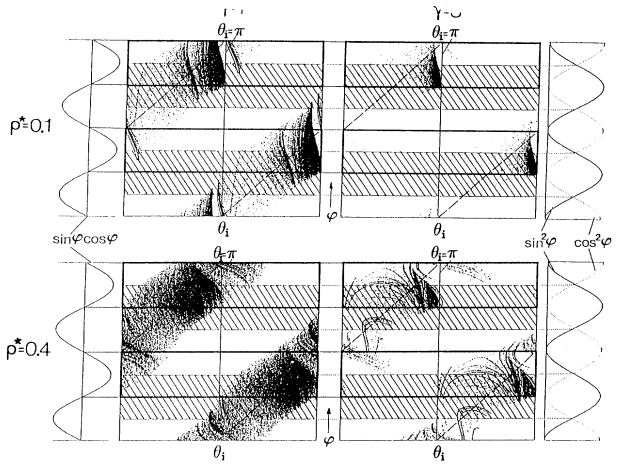

FIG. 6. Qualitative determination of the dependence of the potential part of elements of the pressure tensor from the angular probability distribution of φ and θ_i before the collision at $r=\sigma$. The potential parts of P_{xy}, P_{xx}, and P_{yy} are given by the average value of the products $A(\theta_i,\varphi)\cos\varphi\sin\varphi$, $A(\theta_i,\varphi)\cos^2\varphi$, and $A(\theta_i,\varphi)\sin^2\varphi$, respectively. The values of $\cos\varphi\sin\varphi$ are plotted on the left-hand side of the picture, and the φ intervals where $\cos\varphi\sin\varphi<0$ are framed in a bold frame. They coincide with the φ intervals where the impulse $A(\theta_i,\varphi)$ increases with the shear rate. The functions $\cos^2\varphi$ (dotted line) and $\sin^2\varphi$ (solid line) are plotted on the right-hand side and the φ intervals where $\sin^2\varphi>\cos^2\varphi$ are shaded. The dashed line represents the singular maxima of the impulse. The behavior of the potential parts of P_{xy}, P_{xx}, and P_{yy} can then be estimated from the positions of the maxima of the probability density of θ_i and φ at the collision.

the angle θ between the collisions to rotate towards 0 or π for longer time, and therefore has a similar overall effect on θ_i as the increase in shear rate;

(iii) the increase in shear rate and the decrease in density make the collisions in the second and fourth quadrants of φ more probable then the collisions in the first and third quadrants, and cause the most probable angle φ to move towards $\pi/2$ or $3\pi/2$.

The steady-state probability distribution $f^{\sigma}(\theta_i,\varphi)$ is not a smooth function of θ_i and φ, but rather has a fractal structure [5,9] because the system (1),(2) is dissipative and the phase space trajectory has a sensitive dependence on initial conditions. The simulation results for the potential part of the pressure tensor P_{xy} and the normal stress difference $P_{xx}-P_{yy}$ are presented in Fig. 7. The sign of the potential part of P_{xy} is determined by the sign of the average value of the product $A(\theta_i,\varphi)\cos\varphi\sin\varphi$ at the collision. When shear is present, the collisions in the second and fourth quadrants of φ, where the product is negative, become more probable than the collisions in the first and third quadrants, where it is positive (Fig. 6). For these collisions the impulse contribution to $\langle A(\theta_i,\varphi)\cos\varphi\sin\varphi\rangle$ is also larger, because in the second and fourth quadrants the impulse increases with the shear rate, while in the first and third quadrants it decreases. Therefore the potential part of P_{xy} becomes negative.

The potential part of $|P_{xy}|$ first increases with γ^* because there is an increased probability for the collisions to occur in the second and fourth quadrants, where the impulse $A(\theta_i,\varphi)$ increases with γ^* (Figs. 6 and 7; both densities at shear rate $\gamma^*=1$). When γ^* increases to higher values, the trajectory of the point particle becomes more horizontal and therefore the probability of the collisions in the second and fourth quadrants closer to $\varphi=\pm\pi/2$ increases. The angle θ_i gets closer to $\pm\pi$. The potential part of $|P_{xy}|$ then decreases for two reasons. First, the average value of the impulse $A(\theta_i,\varphi)$ decreases as such values of θ_i and φ become more probable, because the majority of the collisions occur at intervals of $\theta_i-\varphi$ further away from the (singular) maximum. Second, the average value of the product $|\cos\varphi\sin\varphi|$ decreases because $\langle|\cos\varphi|\rangle$ tends to zero when the angles of φ close to $\pm\pi/2$ become favored (Figs. 6 and 7; both densities at $\gamma^*=3$).

The diagonal elements of the potential part of the pressure tensor P_{xx} and P_{yy} depend on $\langle A(\theta_i,\varphi)\cos^2\varphi\rangle$ and $\langle A(\theta_i\varphi)\sin^2\varphi\rangle$, respectively. Their dependence on shear rate can also be accounted for by Fig. 6.

At first both diagonal elements increase with shear rate, because the dominant effects is the increased impulse in the second and fourth quadrants of the collision angle φ, where more collisions take place. Nevertheless, for $\rho^*=0.4$ more collisions occur closer to $\varphi=\pm\pi/2$, where $\sin^2\varphi>\cos^2\varphi$, while the angle θ_i is sufficiently spread out for all angles φ to include values on both sides of the singular maximum in the impulse (Figs. 6 and 7 for $\rho^*=0.4$, $\gamma^*=1$). Therefore the potential part of P_{yy} is

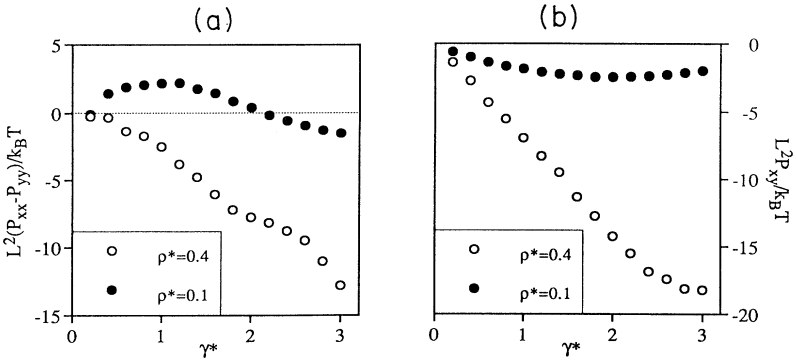

FIG. 7. Potential part of the pressure tensor for hard disks at the reduced densities $\rho^*=0.1$ and $\rho^*=0.4$. (a) The normal stress difference; (b) P_{xy}.

greater than the potential part of P_{xx}. The behavior of the normal stress difference is dominated by the increased probability of collisions close to the top and the bottom of the scatterer, with the larger value of $\sin^2\varphi$.

For $\rho^*=0.1$ (Fig. 6 for $\rho^*=0.1$, $\gamma^*=1$), on the other hand, P_{xx} is greater than P_{yy}. The angle θ_i at the collision has values much closer to π or 0 for the collisions in the φ intervals with $\sin^2\varphi > \cos^2\varphi$. Such a combination of θ_i and φ gives impulses far away from the singular maximum in the impulse. For collisions with $\cos^2\varphi > \sin^2\varphi$ the impulse is much closer to the maximum. Therefore the increased probability of collision angles φ with $\sin^2\varphi > \cos^2\varphi$ is outweighed by their lower contribution to the impulse.

For larger shear rates ($\gamma^*=3$ on Fig. 6) P_{xx} decreases for two reasons: first, there are fewer collisions with $\cos^2\varphi > \sin^2\varphi$; and second, most collisions have the angle θ_i just before the collision close to 0 or π, i.e., far from the maximum. Therefore, as $\gamma\langle\tau\rangle$ becomes large (where $\langle\tau\rangle$ is the average time between the collisions), the potential part of the normal stress difference becomes negative, as opposed to the kinetic part of the normal stress difference.

The results for the potential part of the normal stress difference at different densities (Fig. 7) cannot be described by only one parameter, which implies that the potential part of the pressure tensor depends on density and shear rate as two separate parameters. This is not surprising, since the potential part is determined by the angular distribution $f^{\sigma}(\theta_i,\varphi)$ at the collision and the impulse $A(\theta_i,\varphi)$. Even assuming that the angular distribution depends on a single parameter $\gamma\tau'$, the value of the impulse in the different quadrants of φ (Fig. 5), and the shape of the regions $\dot{r}<0$ over which the averaging is done, depend only on shear rate and not on density.

V. SOFT DISKS

Until recently, only "soft" interactions between particles were used to solve the collisions. When the interaction potential is sufficiently steep at $r=\sigma$, the dependence of the potential part of the pressure tensor on shear rate should be qualitatively similar to this dependence for hard disks.

Soft disks were most frequently simulated using the Lennard-Jones potential truncated at some distance not larger than the length of the periodic cell. We used the Lennard-Jones potential truncated at $r=\sigma$.

$$\phi^{\mathrm{LJ}}=\begin{cases} 4\varepsilon\left[\left[\dfrac{\sigma}{r}\right]^{12}-\left[\dfrac{\sigma}{r}\right]^{6}\right] & \text{for } r<\sigma\ , \\ 0 \quad \text{for } r>\sigma\ , \end{cases} \tag{32}$$

because such a soft-disk Lorentz gas can have the same range of densities as the hard-disk gas. The parameter describing the "softness" of disks with the isokinetic constraint is the "reduced temperature,"

$$T^*=\frac{k_B T}{\varepsilon}=\frac{p^2}{m\varepsilon}\ ,$$

while for the isoenergetic disks the equivalent parameter can be defined as E/ε.

The increase in temperature is manifested as greater "softness" of the scatterers. In all our simulations the reduced temperature was equal to unity.

A. Collisions

The intervals of θ_i around the radial direction described in Sec. III, where hard-disk collisions cannot be solved, persist for soft disks with the isoenergetic constraint (3), but are reduced in size. Nevertheless, a finite fraction of collisions still cannot be solved for soft disks under shear with isoenergetic constraint.

Soft-disk collisions with isokinetic constraint (2), however, can be solved for all shear rates. The impenetrable "hard core" of the soft disks appears more anisotropic at higher shear rates γ^*, as shown in Fig. 8. The black regions consist of dots representing the minimal distances from the origin for a uniform set of angles (θ_i,φ) before the collisions, i.e,. the turning points. The "hard core" is white. For $\gamma^*>4$, in a part of the region where the point particle can move within the scatterer (marked by the dotted line in the picture), there are no turning points. This is the part of the scatterer where the radial component of velocity is always negative and therefore the distance from the center cannot be minimal. This region is enclosed within the "forbidden" (shaded) interval of φ, where a corresponding hard-disk collision could not be solved. The shape of the area enclosed by the dotted lines within the scatterer, where the distance cannot be minimal, does not depend on the form of the repulsive central force, but is determined only by the applied shear rate γ^*.

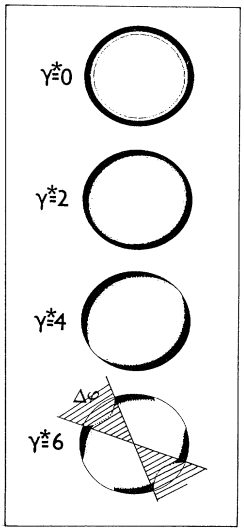

FIG. 8. "Hard core" of soft disks. A uniform distribution of angles (θ_i,φ) before the collision at $r=\sigma$ (along the circumference of the scatterer) is taken as a set of initial conditions for the collision trajectories. The black regions consist of dots representing the minimum distances from the origin (turning points). The hard core of the disk becomes more anisotropic with the increase in shear rate. For $\gamma^*=6$ (i.e., $\gamma^*>4$) the "forbidden" (shaded) intervals of the angle φ appear, where the trajectory can pass but cannot have a turning point.

B. Potential part of the pressure tensor

The collision of soft disks takes place not at a point but over a finite path. The point particle moves through the scatterer during a collision and the kinetic part of the pressure tensor consists of the free-streaming part between the collisions and of the part during the collision. At $T^*=1$ the kinetic contribution of collisions is small compared to the contribution of free trajectories between the collisions, because the repulsive force is sufficiently strong not to allow the point particle to spend too much time within the scatterer. The motion between the collisions obeys the same equations of motion for hard and soft disks, and therefore the dependence of the kinetic part of the pressure tensor on shear rate for soft disks closely resembles the dependence for hard disks, as was found in Refs. [3] and [4].

The dependence of the potential part of the pressure tensor on shear rate for soft disks of reduced densities $\rho^*=0.1$ and $\rho^*=0.4$ is shown in Figs. 9(a) and 9(b), and 9(c) and 9(d), respectively. It is determined by the second term in the rhs of (5), i.e., the average value of $F_\alpha r_\beta$. The angular probability distribution at $r=\sigma$ becomes more disordered than for hard disks, with the less distinct peaks of θ_i for $T^*=1$, but the maxima are still roughly in the same positions in the θ_i,φ plane. Therefore the behavior of the pressure tensor for soft disks is similar to the behavior for hard disks, at least in the range of shear rates $\gamma^*\leq 3$: the normal stress difference is negative for $\rho^*=0.4$ and becomes negative for $\gamma^*>1.5$ for $\rho^*=0.1$. However, the collision impulse for the finite force is less than the impulse for infinitely hard disks (the hard-disk limit of the impulse is approached from below), and this is the main reason why the elements of the potential part of the pressure tensor have smaller absolute values for soft disks than for hard disks.

VI. CONCLUSION

In this paper we investigated the consequences of using isokinetic or isoenergetic constraints in the definition of a hard-disk Lorentz gas system subjected to shear. In equilibrium, the trajectories of the isokinetic and isoenergetic particles were shown to be identical. However, the impulse received by the isokinetic particle is larger than the impulse received by the isoenergetic particle. Therefore the potential parts of the thermostated and unthermostated equilibrium hydrostatic pressures are different, their ratio being equal to 1.831 94. The difference between them comes from the fact that the isokinetic equations (10) are not Newtonian. While for the isoenergetic equations (9) the change of the momentum during the collision is equal to the impulse of the force **F**, this equality is no longer valid for the isokinetic case. The definition of the potential part of the pressure tensor (6) involves the impulse $A(\theta_i-\varphi)$ rather than the total change of momentum $\Delta\mathbf{p}$. The potential part of the pressure tensor therefore gives the contribution of the conservative force of interaction to momentum transfer during a collision. This definition is also consistent with the definition of the kinetic part of the pressure tensor using the peculiar momenta instead of the sum of peculiar and streaming velocities. The alternative definition of the potential part, using $\Delta\mathbf{p}$ instead of A, would yield an asymmetric pressure tensor,

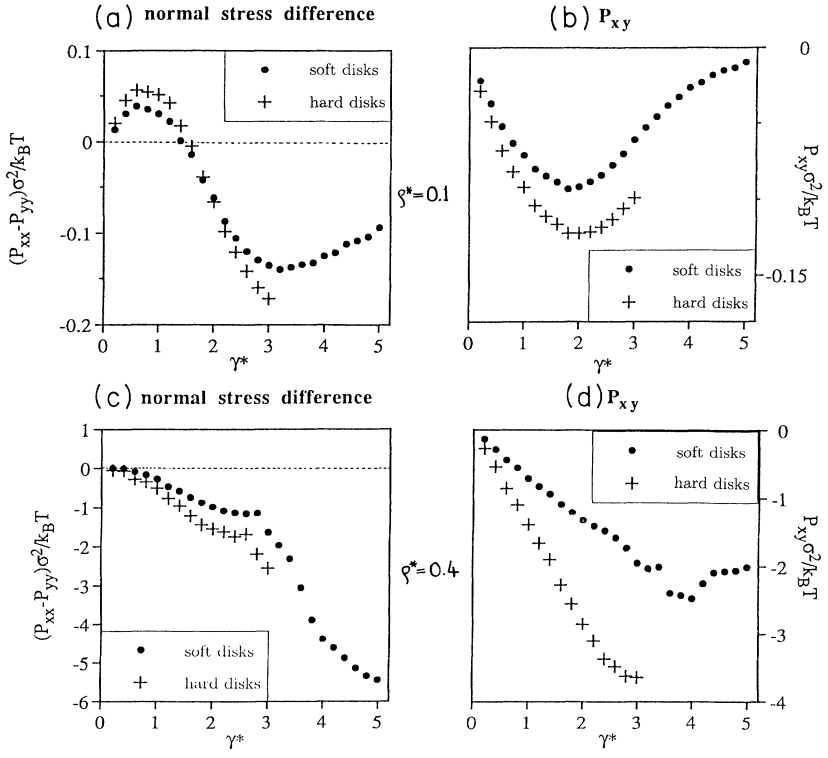

FIG. 9. Potential part of the normal stress difference (a) and the off-diagonal element, (b) of the pressure tensor for soft disks at the reduced temperature $T^*=1$ and hard disks at the reduced density $\rho^*=0.1$. The potential part of the normal stress difference (c) and the off-diagonal element, (d) of the pressure tensor for soft disks of the reduced temperature $T^*=1$ and hard disks at the reduced density $\rho^*=0.4$.

$$P_{xy}^{\text{potential}} \neq P_{yx}^{\text{potential}}$$

for thermostated disks outside equilibrium.

When shear is present, a finite fraction of isoenergetic hard and soft-disk collisions cannot be solved. Therefore the isoenergetic constraint (3) is not appropriate for modeling the Lorentz gas subjected to shear.

The solution of the sheared isokinetic hard-disk collision implies that the magnitude of the radial component of momentum is different before and after the collision, the point particle having a larger radial component after the collision in the quadrants where the radial component of streaming velocity is negative, and a smaller radial component where the radial component of streaming velocity is positive. The impulse in the former case is larger than in equilibrium, while in the latter it is smaller than in equilibrium. The dependence of the impulse on the polar angle of the momentum and the coordinates of the collision point can qualitatively explain the dependence of the potential part of the pressure tensor on shear rate. It can also show that pressure must depend on density and shear rate as separate parameters, implying that the nonequilibrium steady state is characterized by two independent parameters. Similar dependence of the potential part of the pressure tensor on shear rate for soft disks using the Lennard-Jones potential truncated at $r=\sigma$ gives one confidence in the correctness of the collision law for hard disks.

For $\gamma^* > 4$ a fraction of isokinetic hard-disk collisions occurring in the finite interval of the collision angle φ cannot be solved. These "forbidden" collisions are the consequence of using a linear profile thermostat.

The actual probability distribution of the polar angle φ of the collision depends also on density. For very low densities, $\rho^* \ll 0.1$, the collisions are confined to points very close to the top and bottom of the scatterer because of the nearly horizontal trajectories in the vicinity of the scatterer. Therefore for such low densities, the "forbidden" collisions may occur for the first time at the shear rates higher than $\gamma^* = 4$, and the limit of applicability of the linear profile thermostat may be density dependent.

[1] A. W. Lees and S. F. Edwards, J. Phys. C **5**, 1921 (1975).
[2] D. J. Evans and G. P. Morriss, Comp. Phys. Rep. **1**, 297 (1984).
[3] A. J. C. Ladd and W. G. Hoover, J. Stat. Phys. **38**, 973 (1985).
[4] G. P. Morriss, Phys. Lett. **113A**, 269 (1985).
[5] J. Petravic, D. J. Isbister, and G. P. Morriss, J. Stat. Phys. **76**, 1045 (1994); J. Petravic, thesis, University of New South Wales, 1994 (unpublished).
[6] K. W. Kratky and W. G. Hoover, J. Stat. Phys. **48**, 873 (1987).
[7] J. Erpenbeck, Phys. Rev. Lett. **52**, 1333 (1984).
[8] D. J. Evans and G. P. Morriss, Phys. Rev. Lett. **56**, 2172 (1986).
[9] G. P. Morriss, Phys. Rev. A **39**, 4811 (1989).
[10] W. G. Hoover and B. Moran, Phys. Rev. A **40**, 5319 (1989); W. G. Hoover, Physica A **194**, 450 (1993); W. G. Hoover, C. G. Hoover, W. J. Evans, B. Moran, J. A. Levantin, and E. A. Craig, in *Microscopic Simulations of Complex Flows,* NATO Advanced Study Institute Series, edited by M. Mareschal (Plenum, New York, 1990).